PERGAMON

International Journal of Heat and Mass Transfer 46 (2003) 77–89

International Journal of HEAT and MASS TRANSFER

www.elsevier.com/locate/ijhmt

Coalescence collision of liquid drops

F. Mashayek [a,*], N. Ashgriz [b], W.J. Minkowycz [a], B. Shotorban [a]

[a] Department of Mechanical and Industrial Engineering, University of Illinois at Chicago, 842 West Taylor Street 2053 ERF, Chicago, IL 60607, USA

[b] Department of Mechanical and Industrial Engineering, University of Toronto, Toronto, Ont., Canada M5S 3G8

Received 10 May 2002; received in revised form 25 June 2002

Abstract

The coalescence collision of two liquid drops is studied using a Galerkin finite element method in conjunction with the spine-flux method for the free surface tracking. The effects of Reynolds number, impact velocity, drop size ratio, and internal circulation on the coalescence process is investigated. The long time oscillations of the coalesced drop are also studied and curves for the variations of the period and decay factor are provided as a function of the number of oscillations. In the study of non-equal-size drop collision, traces of different fluid particles are calculated to illustrate the liquid mixing during the collision.

© 2002 Elsevier Science Ltd. All rights reserved.

1. Introduction

Liquid drop collision is an important phenomena in atmospheric rain drop formation, and in dispersed phase systems such as dense sprays, liquid–liquid extraction, emulsion polymerization, waste treatment, and hydrocarbon fermentation [1,2]. Due to its significance, drop collision has been the subject of numerous investigations in the past. However, the complexity of this three-dimensional free surface flow problem has limited the full investigation mostly to experiments, and the existing theoretical studies are based primarily on simplified treatments. A detailed review of the experimental studies was provided by Ashgriz and Poo [3] who also presented a theoretical model for the prediction of the boundaries between various collision outcomes. In general, the outcome of the drop collision can be categorized into four different types: bouncing, coalescence, separation, and shattering collisions. Bouncing occurs when the surrounding fluid prevents the touching of the two drops. In this case the drops may go through deformation, however, there is no mass exchange. Coalescence collision occurs at low velocities or low Weber numbers. In this case the two drops combine resulting in a single drop. Separation and shattering collisions are the consequences of higher impact energy collisions. In this paper, due to the limitations of our numerical algorithm, we only consider the coalescence collision among two drops.

The computational studies of drop collision are very limited. One of the first numerical studies was published by Foote [4], who considered the head-on collision of equal-size drops for $We < 5$ using the marker-and-cell method. Poo and Ashgriz [5] used a volume-of-fluid based method (developed by Ashgriz and Poo [3]) to study the collision dynamics of two drops in two-dimensional Cartesian coordinate system. Due to the significant role played by surface tension, the results in this case were very different than the actual three-dimensional problem. Nobari et al. [6] used a front tracking method to simulate the head-on collision of two drops. Their study was focused on the boundary between the coalescence and bouncing. Menchaca-Rocha et al. [7] simulated the binary drop collision using a nuclear-reacting dynamic model developed by Carjan et al. [8]. Their study was aimed at determining the fragmentation condition of the drop collision. A very brief report on the numerical simulation of the drop collision was also published by Riebner and Frohn [9], which mainly discusses the numerical technique and does not provide much details on the collision behavior.

* Corresponding author. Tel.: +1-312-996-1154; fax: +1-312-413-0447.

E-mail address: mashayek@uic.edu (F. Mashayek).

0017-9310/03/$ - see front matter © 2002 Elsevier Science Ltd. All rights reserved.
PII: S0017-9310(02)00256-9

Nomenclature

L	reference length scale
r	radial coordinate
Re	Reynolds number, $\rho UL/\mu$
t	time
u	fluid velocity in z direction
U	reference velocity scale
v	fluid velocity in r direction
w	tangential velocity at the drop surface
We	Weber number, $\rho U^2 L/\sigma$
z	axial coordinate

Greek symbols

μ	viscosity
v	kinematic viscosity
ρ	density
Γ	decay factor
σ	surface tension coefficient

Subscripts

n	oscillation number
CM	center of mass

In this paper we investigate the collision dynamics of two drops using the spine-flux method (SFM) as explained in detail in Mashayek and Ashgriz [10]. We are only able to consider the head-on collision of two drops which allows an axisymmetric representation. We are also limited to surface deformations that do not result in double-definition of the surface along a spine (i.e. a spine cannot intersect the surface at more than one point, otherwise the simulation fails).

2. Formulation and methodology

To study the head-on collision of two spherical drops, we consider the laminar axisymmetric flow of an incompressible Newtonian viscous fluid with constant properties. The governing equations, in non-dimensional form, are described as

$$\frac{\partial u}{\partial z}+\frac{1}{r}\frac{\partial}{\partial r}(rv)=0, \tag{1}$$

$$\frac{\partial u}{\partial t}+u\frac{\partial u}{\partial z}+v\frac{\partial u}{\partial r}-\ddot{z}_{\mathrm{CM}}=-\frac{\partial p}{\partial z}+\frac{1}{Re}\left[\frac{\partial^2 u}{\partial z^2}+\frac{1}{r}\frac{\partial}{\partial r}\left(r\frac{\partial u}{\partial r}\right)\right], \tag{2}$$

$$\frac{\partial v}{\partial t}+u\frac{\partial v}{\partial z}+v\frac{\partial v}{\partial r}=-\frac{\partial p}{\partial r}+\frac{1}{Re}\left[\frac{\partial^2 v}{\partial z^2}+\frac{1}{r}\frac{\partial}{\partial r}\left(r\frac{\partial v}{\partial r}\right)-\frac{v}{r^2}\right]. \tag{3}$$

Here, all lengths are normalized by the initial radius of the larger drop, and the reference velocity is chosen such that $We=1$. It is noted that for collision of non-equal-size drops, the origin of the coordinate system is not necessarily coincided with the CM. Therefore, the body force generated by the acceleration of the CM has to be included in the momentum equation. However, owing to the axial symmetry, the CM always remains on the z-axis and the body force due to the acceleration of the CM is only included in the momentum equation in the axial direction. This term is shown by $\ddot{z}_{\mathrm{CM}}$ in Eq. (2).

Both pressure and viscous effects, along with surface tension, are included in the description of boundary conditions at the surface of the drop. The implementation of these boundary conditions, in conjunction with a Galerkin finite element method, is described in [10] and will not be repeated here for brevity. The free surface is tracked using the SFM of Mashayek and Ashgriz [10]. Here we present only a brief description of SFM, and refer to [10] for details. To follow the motion of the free surface, the fluid domain is divided into small subvolumes which are separated by spines as shown in Fig. 1a. The location of the interface is given by its distance from the origin of the coordinate system along these spines. At the end of each time step fluxes of the fluid from each subvolume to its neighboring subvolumes are calculated using the velocity field as determined by the finite element solution of the governing equations. After the new volume of the fluid in each subvolume is calculated, a linear approximation is used to describe the part of the free surface confined within every pair of neighboring subvolumes. With the knowledge of the volumes of fluid inside these subvolumes, the constants of the line are determined and the intersection of the free surface with the common spine between the neighboring subvolumes is obtained. Repeating this procedure for all the spines yields the location of the free surface which is then used to generate a new finite element mesh for the next time step.

In the collision of non-equal-size drops, the asymmetric evolution of the surface may result in a surface shape that becomes very close to the origin of the coordinate frame from one side (Fig. 1b). In more severe cases the surface may even pass the origin, resulting in a situation where no unequivocal radial direction exists. Obviously, when this happens, calculations become considerably less accurate, if not impossible, unless a measure is adopted to shift the coordinate from its

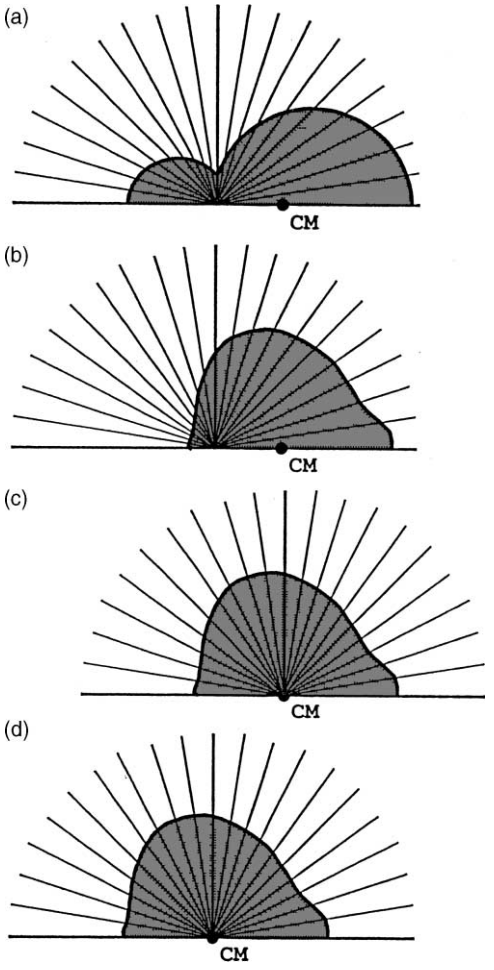

Fig. 1. The coordinate shift procedure is explained by using schematics of a drop collision problem. (a) In the initial set-up of the problem the coordinate is located on the contact surface of drops which is not coincided with the CM of the system. (b) After coalescence the liquid drop oscillates about the CM which results in improper discretization of the liquid domain into subvolumes. To achieve the proper discretization, either (c) the coordinate origin is shifted to the CM or (d) the CM is shifted to the origin of the coordinate system.

original position. One way to accomplish this task is to consider an artificial motion of the liquid domain relative to the coordinate. This process is guaranteed not to affect the solution, due to the invariance of the Navier–Stokes equations under a Galilean transformation. Therefore, initially a constant axial velocity is added to the liquid velocity field which results in a relative motion of the liquid domain with respect to coordinate. The magnitude of this velocity is chosen such that it results in a proper coordinate shift during the expected time interval. Once the coordinate is reached to its desired position the constant velocity is subtracted from the velocity field. This procedure is shown schematically in Fig. 1 and explained in more details in [10].

3. Effect of Reynolds number

In this section we will investigate the effect of variation of the Reynolds number on the outcome of the head-on collision of two equal-size drops. The maximum *Re* that we could reach without a failure of the surface reconstruction technique is 60. The initial non-dimensional relative velocity, $u_{\mathrm{rel}} = 2$, is held constant for all cases and the Reynolds number is varied in the range $3 \leqslant Re \leqslant 60$. For water drops with density $\rho = 10^3$ kg/m^3, kinematic viscosity $\nu = 10^{-6}$ m^2/s, and surface tension coefficient $\sigma = 0.067$ N/m, the case with $Re = 60$ corresponds to a drop radius of 54 μm and a dimensional initial relative velocity of 2.23 m/s. A 30×9 finite element mesh is used for the simulations and the time increment, δt, is chosen based on the value of *Re*.

Shown in Fig. 2a–c is the temporal evolution of the collision for the drops with $Re = 5$, 30, and 60. To initiate the simulations a small initial contact is assumed between the drops and due to the symmetry only a quarter of the shapes shown in the figures is considered. The early stages of collision ($t < 6.5$) are mainly governed by the initial kinetic energies of the drops as well as the presence of a very large surface curvature at the interface between them. The former results in uniform motion of the end parts of the drops toward each other along the *z*-axis, while the latter causes a fast outward motion of the surface along the *r*-axis.

The curves representing the motion of the surface points which are located on the *z* and *r* axes are shown in Fig. 3a and b for different *Re*. It is clearly seen in Fig. 3a that the motion of the surface point on the *z*-axis is independent of *Re*, during the time interval $t < 6.5$. The motion of the surface point on the *r*-axis, however, is more sensitive to the variation of the Reynolds number and slows down as *Re* is decreased (Fig. 3b). This behavior can be explained by considering the fact that since the Weber number and the initial impact velocity are kept constant, variation of *Re* is inversely proportional to changes of viscosity, μ. Therefore, a case with lower *Re* corresponds to a drop with higher viscosity while all other parameters remain the same. It is also known that, the viscous effects are proportional to velocity gradients, not to the velocity itself; i.e., the higher the velocity gradients, the larger the viscous effects. In the end parts of the drops, around the *z*-axis, velocities are mostly parallel to the axis and of similar magnitudes, during the early stages of collision. As a result, smaller viscous effects are experienced in these parts of the drops. The fluid motion near the *r*-axis, however, must

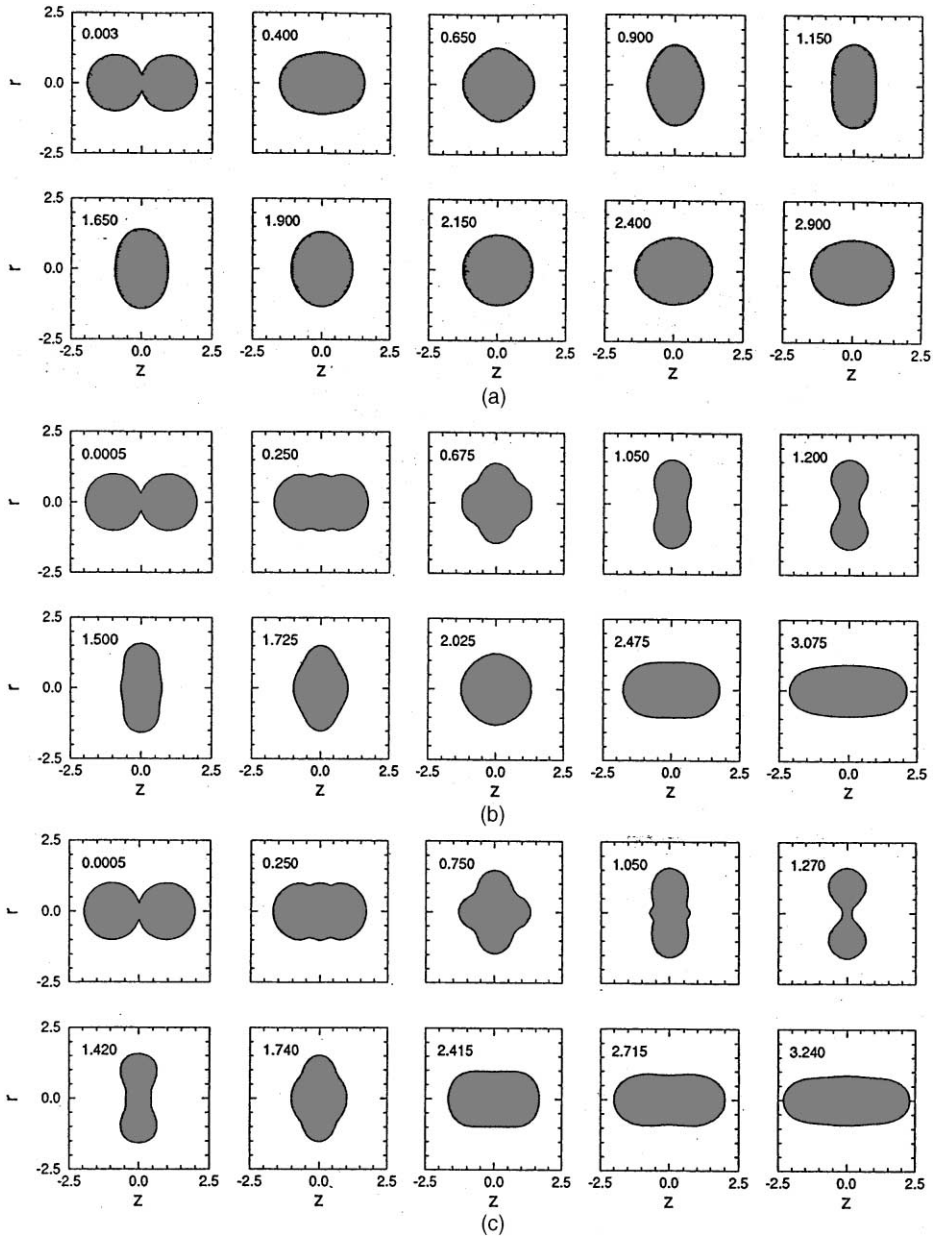

Fig. 2. Time resolved shape evolution of the head-on collision of two equal-size drops with $u_{rel} = 2$: (a) $Re = 5$, (b) $Re = 30$, and (c) $Re = 60$. The numbers on the figure represent the time.

experience a sharp turn from the axial to the radial direction. Also, the magnitude of the velocity in this region changes quickly due to the high surface energies involved. Consequently, the fluid motion experiences larger viscous effects along the r-axis as compared to that along the z-axis.

The first major effect of the Reynolds number variation on the motion of the surface point along the z-axis is observed during $6.5 < t < 8$ when the curves shown in Fig. 3a start to separate. As the Reynolds number is increased, the motion of the surface at the end parts of the drops slows down and for $Re > 40$ reverse motions are recorded for these parts. A similar phenomenon has previously been observed in the oscillation of a single drop [10,11]. In fact, the same argument can explain this reverse motion. Fig. 2c shows

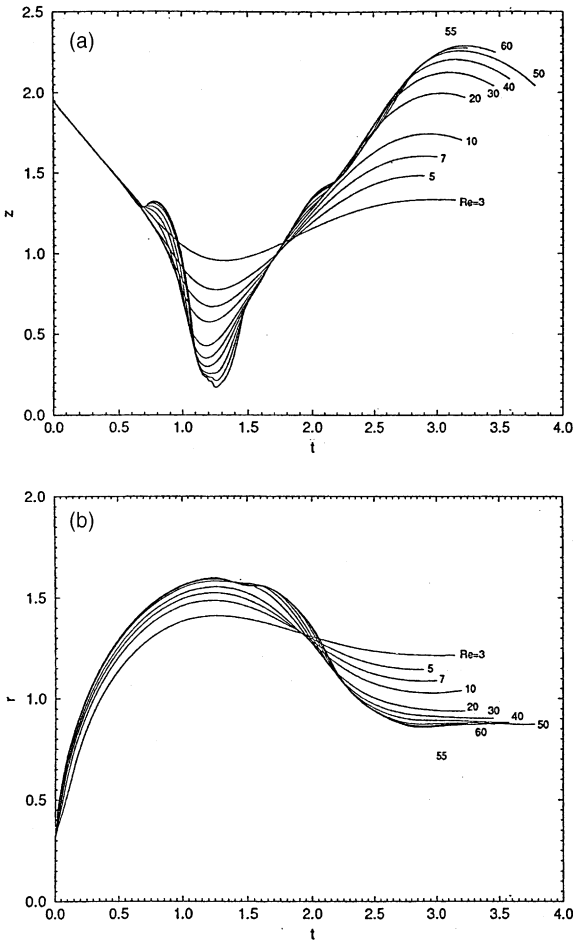

Fig. 3. Motion of the surface point located on the (a) z-axis (b) r-axis for different Reynolds numbers in head-on collision of two equal-size drops with $u_{rel} = 2$.

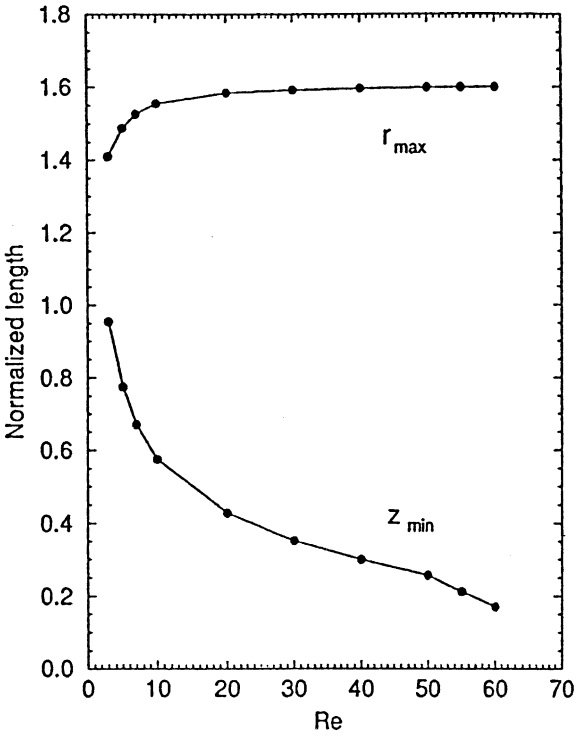

Fig. 4. Variation of the minimum thickness along the z-axis, z_{min}, and maximum radius, r_{max}, reached in the head-on collision of two equal-size drops as a function of Reynolds number. The impact velocity is $u_{rel} = 2$.

that, at $t = 0.75$, a large concave surface is formed around the spine which is at 45° with respect to the z-axis. The formation of this concave surface prevents the motion of the drop surface along the z-axis by pushing the fluid towards the axis of symmetry. Notice that at low Reynolds numbers, no such a concave surface is formed (see Fig. 2a.)

The last slides in top rows of Fig. 2a–c show the coalesced drops in their maximum surface deformation situation for various Reynolds numbers. As expected, higher *Re* values result in larger surface deformations. The portion of the surface around the z-axis continues to move inward due to its initial kinetic energy, until it is faced with the adverse effects of the surface energy in this area. The concave surface around the z-axis produces adverse pressures which tend to prevent further inward motions of the surface. From a numerical point of view, this is the critical situation where higher Reynolds numbers result in the failure of the surface reconstruction technique. The maximum surface deformation that has been successfully simulated is seen in Fig. 2c for $Re = 60$ at $t = 1.27$. A close inspection of Fig. 3a and b reveals that both surface points along the z and r axes experience small slow downs in their motions close to the maximum surface deformation situation for $Re > 50$. In Fig. 4 we have shown the minimum thickness (z_{min}) and maximum radius (r_{max}) of the surface reached during the simulations as a function of *Re*. It is clearly observed that a decrease of *Re* substantially increases z_{min} while reducing r_{max}. It is also seen in Fig. 4 that the curve for z_{min} shows a change of slope for $Re > 50$.

The lower rows of slides in Fig. 2a–c show the reverse motion of the surface toward the completion of the first period of oscillation. The last slide of each figure depicts the coalesced drop close to the end of its first period of oscillations. Higher Reynolds number collisions result in more elongated drops along the z-axis. We have also calculated the period of the first oscillation based on the maximum value obtained for the parameter s which is defined as the ratio of the surface location along the z-axis to that along the r-axis. The variation of the first period with *Re* is given in Fig. 5. Two minima are noted

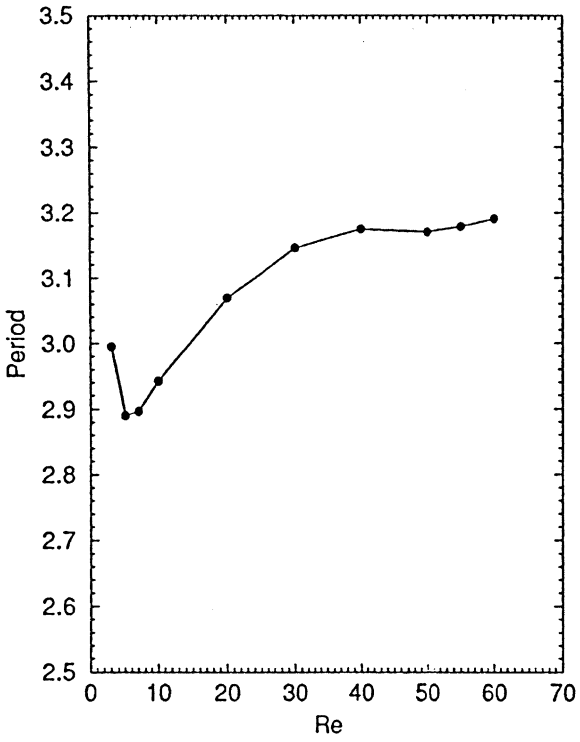

Fig. 5. Variation of the first period of oscillation in head-on collision of two equal-size drops as a function of Reynolds number. The impact velocity is $u_{rel} = 2$.

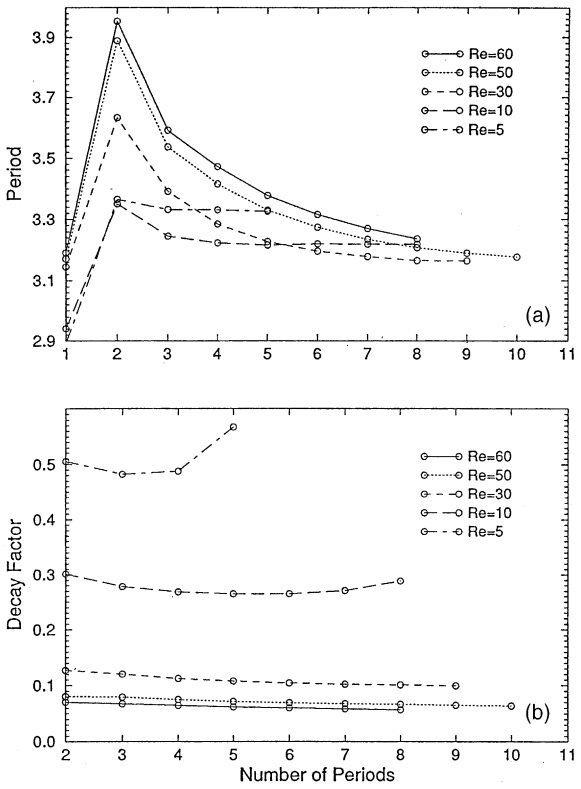

Fig. 6. Variation of (a) period and (b) decay factor with number of periods for the head-on collision of two equal-size drops.

on the curve, one at $Re = 5$ and the other at $Re = 50$. The latter is explained by considering the slow-downs occurred in the motion of the surface point along the z-axis for $Re > 50$ (see Fig. 3a). The occurrence of the minimum at $Re = 5$ should be attributed to the surface energy of the drop at maximum surface deformation position. Fig. 2a at $t = 1.15$ shows that with $Re = 5$ no concave curvature is formed around the z-axis. Therefore, this part of the surface tends to decelerate the reverse flow rather than to accelerate that which is the case with higher Reynolds numbers. The larger period of oscillation at $Re = 3$ is due to the increase of the viscous effects as the Reynolds number is decreased.

For cases with $Re = 5$, 10, 30, 50, and 60 simulations are continued for longer times until oscillations of the combined drop fall within the linear region; i.e. the amplitude of oscillations becomes less than 10% of the radius of an equivalent spherical drop [12]. Shown in Fig. 6 is the variation of the period of oscillation versus the number of periods. The first period of oscillation, which also includes the coalescence process, is considerably smaller than the second period for all Reynolds numbers. This is due to the initial kinetic energy of the drops which accelerates the surface deformation during the first half-period (see Fig. 2a–c). The second period of oscillation is the longest one for all Reynolds numbers and then the periods begin to decrease. For $Re = 30$, 50, and 60 the decreasing trend continues throughout the simulation time, however, for $Re = 10$ a minimum is observed at the fifth period which is followed by an increase in period. We have also calculated the decay factor for the oscillations using the relation

$$\Gamma_n = \frac{1}{\tau_n} \ln\left(\frac{s_n - 1}{s_n}\right),$$

where Γ_n is the decay factor and τ_n is the period for the oscillation number n. The variation of the decay factor, for different Reynolds numbers, with the number of periods is shown in Fig. 6b. A minimum in the curve is observed for $Re = 5$ and 10 while curves for $Re = 30$, 50, and 60 decrease continuously.

4. Collision of sheared drops

There are many practical situations in which liquid drops are subjected to a tangential surface shear, e.g. a

rain drop falling through the atmosphere or a drop breaking off its parent liquid. The presence of a surface shear could result in internal flows affecting the behavior of the drop [11]. Furthermore, if thermocapillary effects are involved even stronger flows are induced inside drops [13]. In this section, we wish to study the collision of drops which have already been subjected to tangential shear stress on the surface. In order to generate the internal flows, we first consider a constant-magnitude tangential velocity, w, on the free surface as the boundary condition. To satisfy the symmetry conditions the surface velocity is assumed to be zero on the z-axis. Once the flow field inside the drop reaches a steady state, it is used as the initial velocity field to study the collision of the drops. At this point, the time is reset to zero ($t = 0$) and the tangential surface velocity is removed.

Three initial surface velocities are considered, i.e. $w = -0.5$, 0, 0.5 for drops with $Re = 50$ and $u_{rel} = 2$. Only equal-size drops are studied here. Fig. 7a and b shows the velocity field inside the drop before the collision, observed in a coordinate system attached to the CM of the combined drops. The impact velocity in this coordinate system is equal to unity for each drop, therefore, in the absence of the surface shear, the velocity field would have been described as $u = -1$ and $v = 0$ for the drop shown in Fig. 7. The application of the surface velocity $w = 0.5$ induces a clockwise circulation inside the drop, and superposition of this velocity field on the impact velocity results in an initial velocity field as seen in Fig. 7b.

Shown in Fig. 8a and b are the time evolution of the surface for cases with $w = 0.5$ and -0.5, respectively. A comparison of the slides which belong to equal times reveal the differences in the shape evolution. For example, at $t = 0.7$ a flat region around the z-axis is seen for the drop with $w = -0.5$ in Fig. 8b. The shape of the coalesced drop when it attains its minimum thickness along the z-axis is shown in Fig. 8a and b at $t = 1.20$ and 1.25 for drops with $w = 0.5$ and -0.5, respectively. It is clearly seen that a clockwise internal circulation (generated by a positive surface velocity) results in a thinner drop and at an earlier time (1.20 versus 1.25).

In Fig. 9a and b we have plotted the motion of the surface points which are located on z and r axes, respectively. An inspection of this figure, and also Fig. 8a and b, reveals that the surface evolution is not significantly affected by the internal circulation for $t < 0.6$. Fig. 9a shows that at $t = 0.6$ the curves start to separate. Although, for all cases a backward motion is observed for the point on the z-axis, this motion is more visible for the case with $w = 0.5$. This is contrary to the fact that a positive surface velocity produces an initial velocity along the z-axis toward the center of the drop and indicates that the fluid which is pushed along the z-axis is substituted by the fluid pushed toward the z-axis in the radial direction.

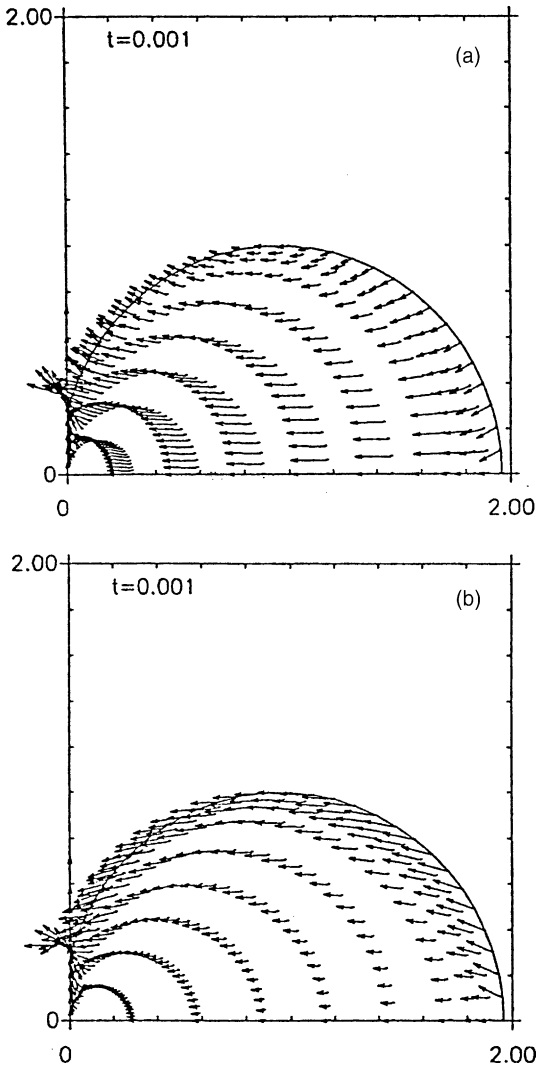

Fig. 7. Initial velocity fields used for the simulation of the sheared drop collision; $Re = 50$, $u_{rel} = 2$: (a) $w = 0.5$ and (b) $w = -0.5$.

The variations of the period of oscillation and the decay factor with the number of periods were also studied (not shown here). The results showed that the period of oscillation is the largest for $w = 0$. Therefore, the addition of the internal circulation results in a decrease in the period, irrespective to the direction of the circulation. Nevertheless, a counterclockwise circulation decreases the period of oscillation more than a clockwise circulation having the same magnitude. It was also found that at long times, as the effects of the initial circulation disappears, the periods of oscillation for different cases approach the same value.

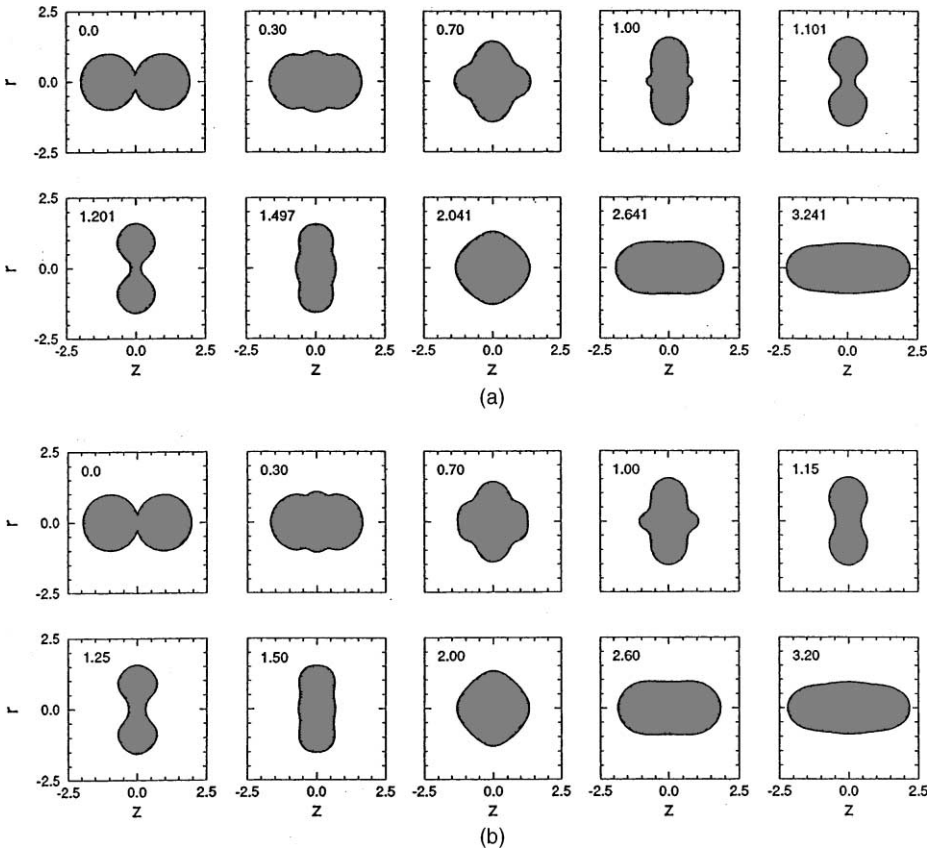

Fig. 8. Time resolved shape evolution of the head-on collision of two sheared equal-size drops with $Re = 50$ and $u_{rel} = 2$: (a) $w = 0.5$ and (b) $w = -0.5$.

5. Effect of drop size ratio

In this section, we consider the collision of non-equal-size drops. As pointed out in Section 2, the study of this case becomes more complicated since the velocity of the CM is not constant for the collision of non-equal-size drops. Furthermore, the surface experiences large deformations which can be captured by using a coordinate shift technique as explained in Section 2.

The first set of simulations considered here, investigates the effect of variation of the impact velocity on the outcome of the collision of two drops with the size ratio $\Delta = 0.5$. The size ratio Δ is defined as the ratio of the radius of the smaller drop to that of the larger drop. The Reynolds number is held constant at $Re = 50$ for all simulations. Four cases with $u_{rel} = 0$, 1, 2, and 3 have been considered. In Fig. 10a and b we have shown the temporal evolution of the surface for the two limiting cases with $u_{rel} = 0$ and 3, respectively. All of the results are presented on a coordinate system that moves with the initial velocity of the CM. In Fig. 10b, surface shapes are given in smaller time intervals during the initial stages of collision, therefore, details of the coalescence process are more clearly seen in this figure. As expected, a larger impact velocity results in a larger penetration of the smaller drop inside the larger one. A comparison of the figures at identical times reveals the effect of the impact velocity. In the very early times, the large surface curvature formed at the contact plane pushes the surface outward and the largest surface deformations are observed in this region (compare the slides at $t = 0.08$). Later, the kinetic energy effects become dominant and the surface shapes for the smaller drop differs dramatically based on the impact velocity. For example, a comparison of the surface shapes at $t = 0.26$ (for the case with $u_{rel} = 3$ consider $t = 0.255$) shows that the small drop is about to being completely absorbed into the larger drop for $u_{rel} = 3$ while it remains virtually intact for the case with $u_{rel} = 0$. After the completion of the coalescence process, the combined drop begins to oscillate non-symmetrically. The amplitude of the oscillation is larger for the case with higher impact velocity.

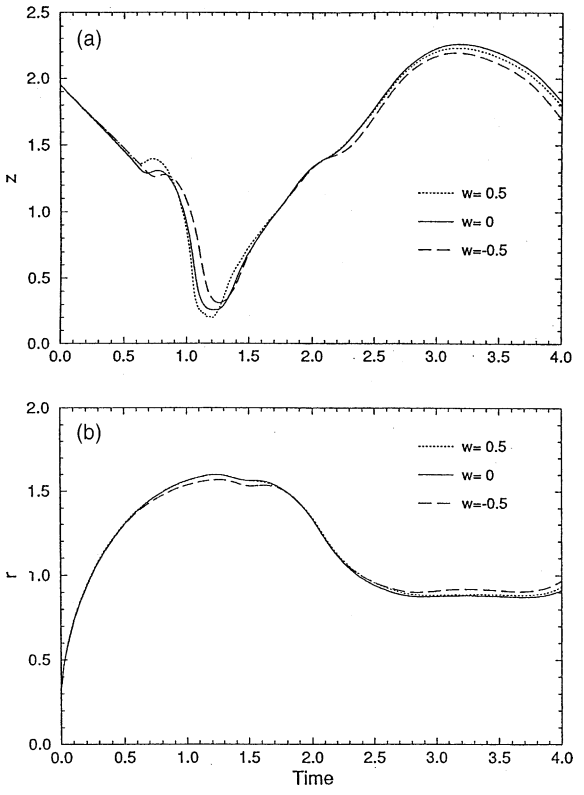

Fig. 9. Motion of the surface point located on the (a) z-axis (b) r-axis for different surface velocities in head-on collision of two sheared equal-size drops with $Re = 50$ and $u_{rel} = 2$.

In Fig. 11a and b we have shown the surface evolution for collision of drops with $\Delta = 0.7$ and 0.9, respectively. For both cases $Re = 50$ and $u_{rel} = 2$. Fig. 11b shows that even a small deviation from $\Delta = 1$ results in a highly non-symmetric coalescence process. In general, for all the cases studied here, irrespective to the impact velocity and drop size ratio, the early stages are characterized by larger surface deformations of the smaller drop. After the surface of the combined drop reaches its maximum deformation on the side of the smaller drop, then the other side of the surface approaches its maximum deformation. As a result, the surface points on the z-axis oscillate with a phase shift. To further demonstrate this point, in Fig. 12 we present the temporal variations of the radii of the drop along the z-axis on the sides of the smaller (- - -) and the larger ($\cdots$) drops. It is also noted that, at longer times when the oscillations of the combined drop decays and the drop approaches a spherical shape, the phase shift is eliminated.

An important issue in the study of drop collision is the extent of mixing of the fluids that form each initial drop. Although in this study we have made no distinction between the liquids in the two drops, an investigation into the mixing process can be conducted by considering the traces of fluid particles. In Fig. 13 we have shown fluid particle traces for the two cases considered in Fig. 11. The trace is found by following the particle in a Lagrangian frame. At each time step the velocity of the particle is calculated by interpolating the Eulerian node velocities using the finite element isoparametric mapping. Then the particle is moved to its new location using the following explicit scheme:

$$z_i(t + \delta t) = z_i(t) + u_i \delta t$$

$$r_i(t + \delta t) = r_i(t) + v_i \delta t$$

where u_i and v_i denote the velocity of the particle i in axial, z, and radial, r, directions, respectively.

A total of six particles are considered in each case, three are initially located near the axis of symmetry and three others are close to the free surface. Also shown on the figures is the initial configuration of the drops which clearly specifies the relative locations of the particles at $t = 0$ shown by (●). As expected, there is a larger penetration into the larger drop at smaller size ratios. It is also clear that the major portion of the penetration occurs in the short initial interval $t \leqslant 1$, during which the coalescence process is in progress. For $t > 1$, the motion of the fluid particles is mainly oscillatory and the net displacement may not be as large as in $t \leqslant 1$ period.

6. Conclusion

The head-on collision of two liquid drops is studied using the SFM of Mashayek and Ashgriz [10]. Only the coalescence collision is considered and the effects of the Reynolds number, drop size ratio, impact velocity, and internal circulation on the behavior of the combined drop are investigated. In collision of equal-size drops, an increase of the Reynolds number results in increasingly thinner drops during the coalescence process. When collision of non-equal-size drops is considered, the early stages of coalescence involves considerably larger deformations for the smaller drop. A study of the motion of the drop surface along the axis of symmetry reveals that the two ends of the combined drop begin to oscillate with a phase shift for collision of non-equal-size drops. At longer times, the drop approaches a spherical shape and the phase shift is eliminated. The period of oscillations for the combined drop is also measured and it is found that the first oscillation period is always shorter than the second period, regardless of the Reynolds number. The effects of an initial internal circulation within the drops are also investigated and the differences in shape evolution and period of oscillations are highlighted. These effects are primarily contained within the first few oscillations.

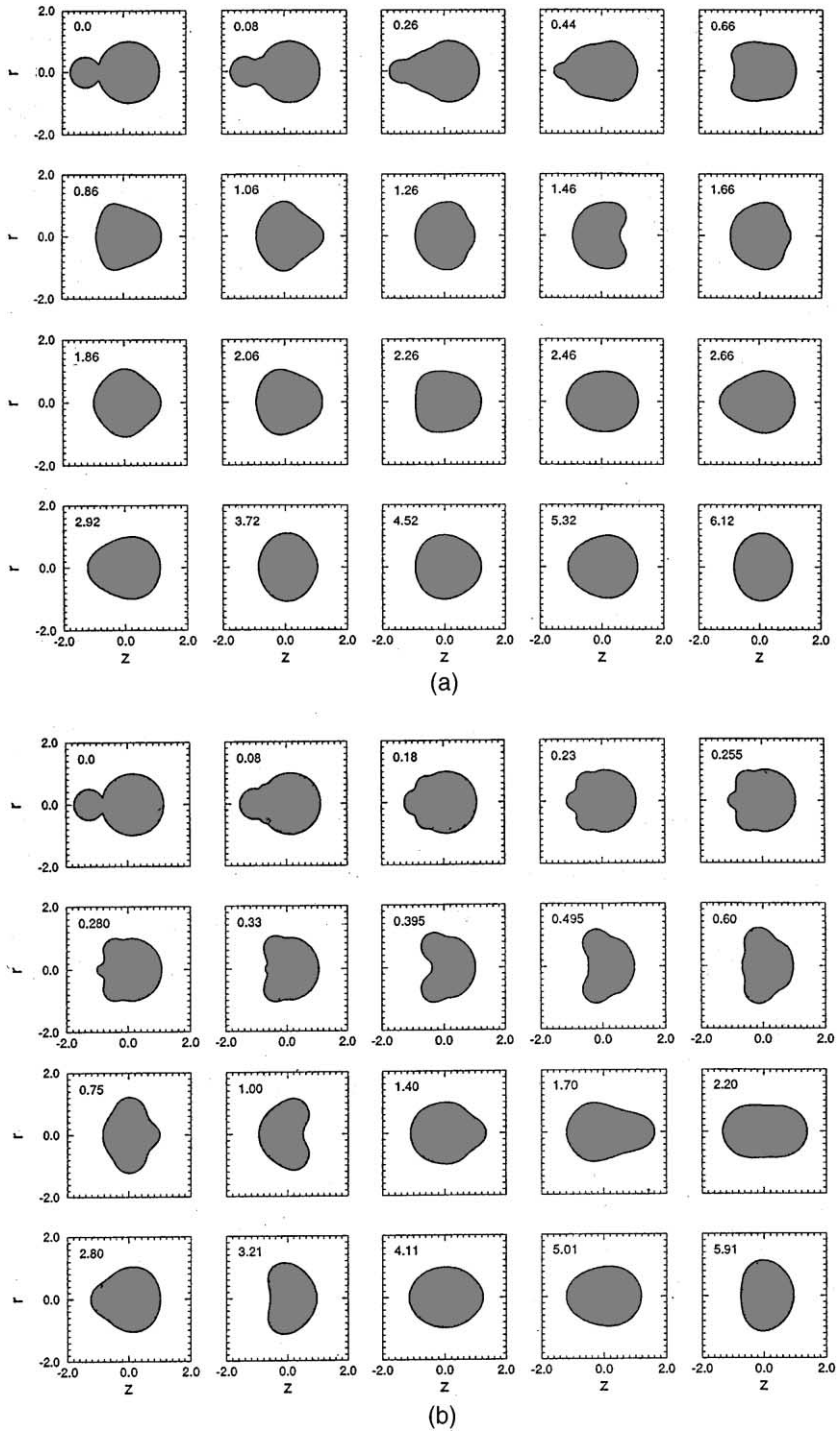

Fig. 10. Time resolved shape evolution of the head-on collision of two drops with size ratio $\Delta = 0.5$ and $Re = 50$: (a) $u_{rel} = 0$ and (b) $u_{rel} = 3$.

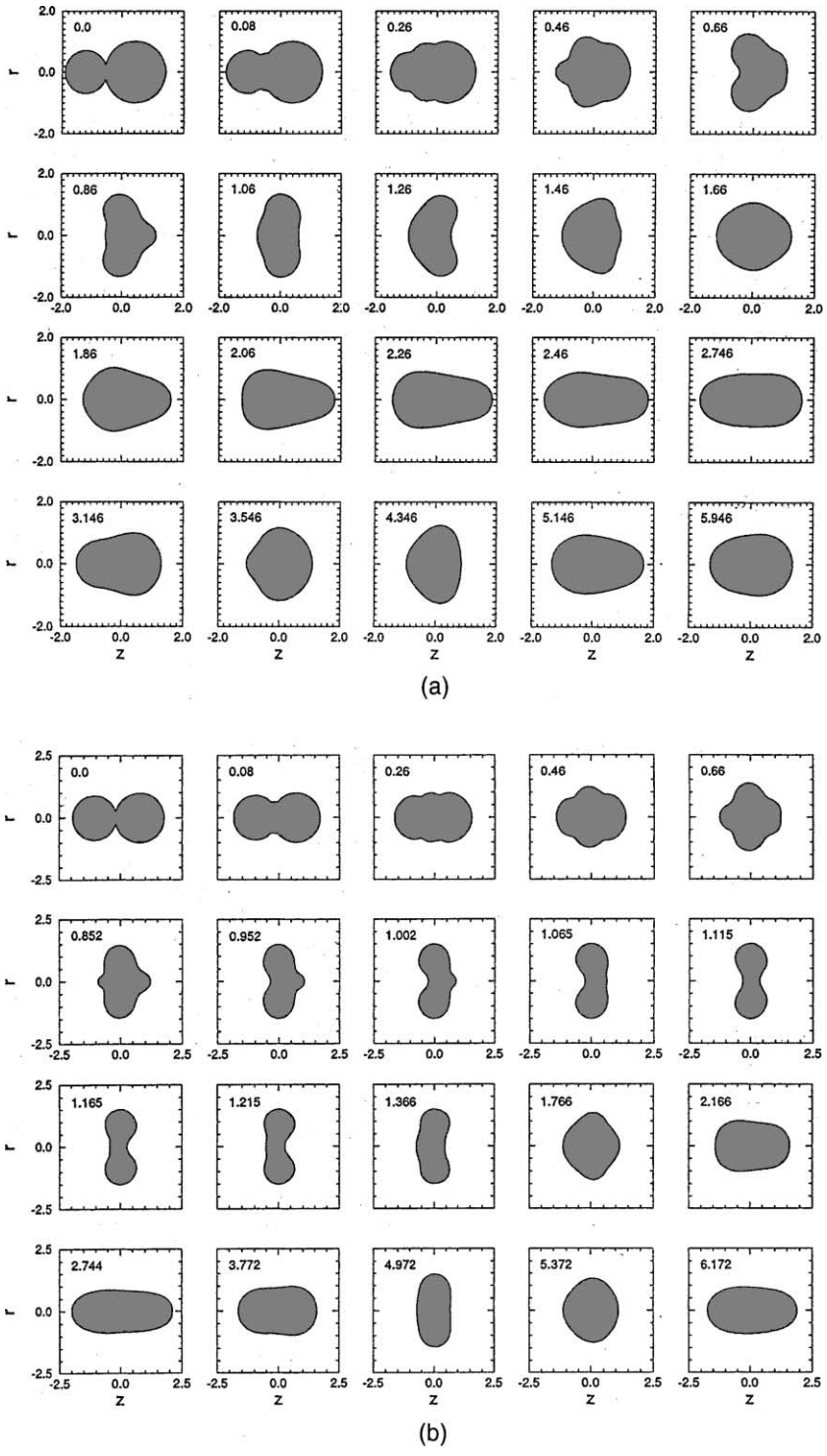

Fig. 11. Time resolved shape evolution of the head-on collision of two drops with $Re = 50$ and $u_{rel} = 2$: (a) $\Delta = 0.7$ and (b) $\Delta = 0.9$.

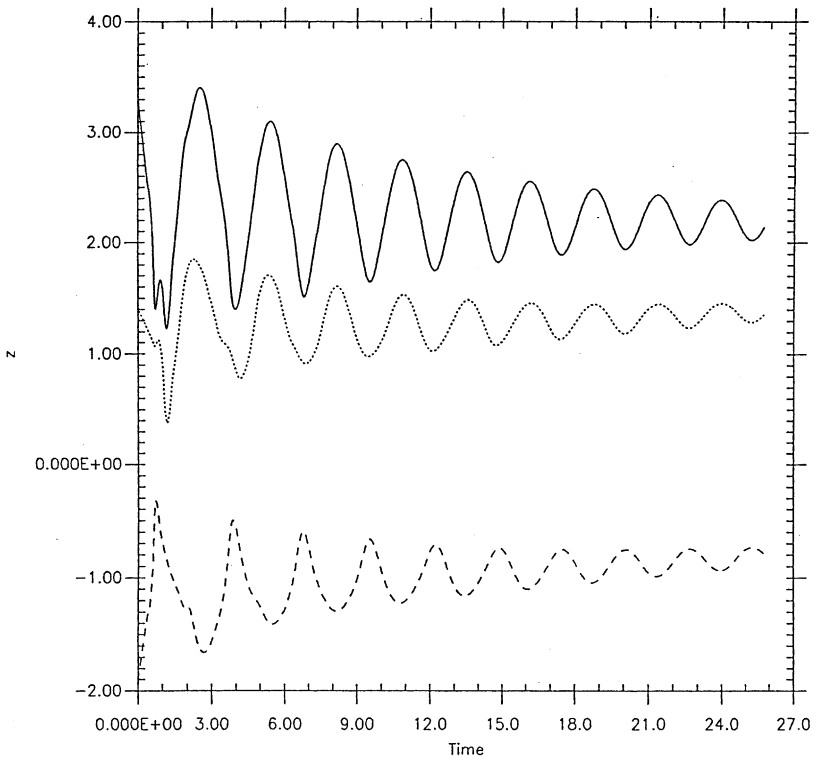

Fig. 12. Motion of the surface point located on the z-axis (- - -) on the smaller drop side and ($\cdots$) on the larger drop side. (—) shows the difference between the two curves. $Re = 50$, $u_{rel} = 2$, and $\Delta = 0.7$.

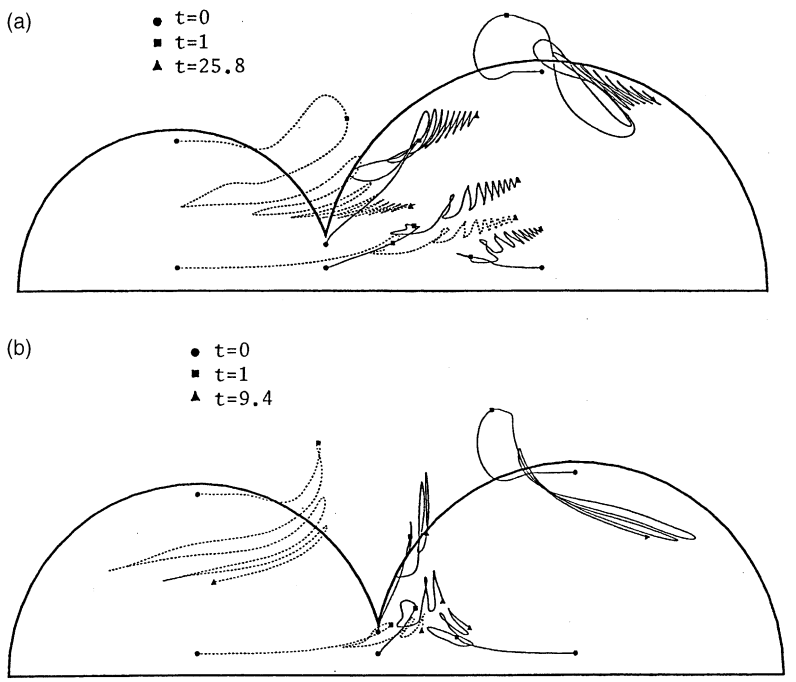

Fig. 13. Lagrangian particle traces for six different particles in head-on collision of drops with $Re = 50$ and $u_{rel} = 2$: (a) $\Delta = 0.7$ and (b) $\Delta = 0.9$.

Acknowledgements

This work was supported in part by the Office of Naval Research and the National Science Foundation.

References

[1] P.S. Shah, L.T. Fan, I.C. Kao, L.E. Erickson, Modeling of growth processes with two liquid phases: A review of drop phenomena, mixing, and growth, Advances in Applied Microbiology (1972).

[2] P.J. O'Rourke, F.V. Bracco, Modeling of drop interactions in thick sprays and a comparison with experiments, in: Stratified Charge Auto Engineering Conference, Institute of Mechanical Engineering Publications, 1980, 101 ISBN 0-85298-4693.

[3] N. Ashgriz, J. Poo, Coalescence and separation in binary collisions of liquid drops, J. Fluid Mech. 221 (1990) 183.

[4] G.B. Foote, The water drop rebound problem dynamics of collision, J. Atmos. Res. 32 (1975) 390–401.

[5] J.Y. Poo, N. Ashgriz, Numerical simulation of collision of two-dimensional drops, in: Proceedings of the Fifth Annual Conference on Liquid Atomization and Spray Systems, San Ramon, CA, 1992.

[6] M.R.H. Nobari, Y.J. Jan, G. Tryggvason, Head-on collisions of drops—A numerical investigation, Phys. Fluids 8 (1) (1996) 29–42.

[7] A. Menchaca-Rocha, M. Borunda, S.S. Hidalgo, F. Huidoboro, K. Michaelian, V. Rodriguez, Search for exotic shapes in liquid-drop collisions, in: The Proceedings of the 12th Winter Workshop on Nuclear Dynamics, Advances in Nuclear Dynamics, Snowbird, UT, 1996.

[8] N. Carjan, A.J. Sierk, J.R. Nix, Effect of dissipation on ternary fission in very heavy nuclear systems, Nucl. Phys. A 452 (1986) 381–397.

[9] M. Riebner, A. Frohn, Navier–Stokes simulations of droplet collision dynamics, in: Proceedings of the Seventh International Symposium on Computational Dynamics, Bejing, China, 1997, pp. 520–525.

[10] F. Mashayek, N. Ashgriz, A spine-flux method for simulating free surface flows, J. Comput. Phys. 122 (1995) 367–379.

[11] F. Mashayek, N. Ashgriz, Nonlinear oscillations of drops with internal circulation, Phys. Fluids 10 (5) (1998) 1071–1082.

[12] E. Becker, W.J. Hiller, T.A. Kowalewski, Experimental and theoretical investigation of large amplitude oscillations of liquid droplets, J. Fluid Mech. 231 (1991) 180–210.

[13] B.S.C. Lau, F. Mashayek, Dynamics of oscillating drops with thermocapillary flows, Theor. Comput. Fluid Dyn. 14 (2001) 203–222.